Int. J. Heat Mass Transfer. Vol. 24. No. 10, pp. 1589 1597. 1981
Printed in Great Britain

0017 9310/81/101589 09 $02.00/0

FREE-FORCED LAMINAR FLOW CONVECTIVE HEAT TRANSFER FROM A SQUARE CAVITY IN A CHANNEL WITH VARIABLE INCLINATION

J. A. C. HUMPHREY and E. W. JACOBS*
Department of Mechanical Engineering, University of California, Berkeley, CA 94720, U.S.A.

(*Received* 9 *October* 1980 *and in revised form* 24 *March* 1981)

Abstract—Free-forced laminar flow convective heat transfer from a square cavity in a channel with variable inclination has been investigated numerically using Boussinesq approximated equations. All walls of the geometrical configuration are adiabatic except for the back wall in the cavity which was kept at a constant temperature higher than that of the entering flow. The influence on heat transfer of cavity orientation, channel inclination, flow direction and entrance profile have been studied for flow conditions corresponding to $Pr = 0.709$, $Re = 300$ and $Gr = 4500$; based on the cavity width, mean flow rate and a cavity orientation angle $\gamma = 0$ corresponding to vertical channel flow.

The calculations show that significant buoyant forces arise in the cavity where $Gr/Re^2 \simeq 30$ but that these are small in the channel where $Gr/Re^2 \simeq 0.05$. In general, the calculations show enhanced rates of heat transfer when buoyant forces are opposed to the main flow direction and diminished rates of heat transfer when they are aligned in the same direction.

Stable stratification of the flow in a downward-facing cavity geometry is responsible for reducing the rate of heat transfer relative to an upward-facing geometry under equivalent flow conditions.

Although limited to a narrow range of geometric and dynamic characteristics wherein the Boussinesq approximation applies, the present results show clearly the relative roles and magnitudes of these effects and should therefore be of value to researchers concerned with the influence of buoyancy driven motions in ducted flows.

NOMENCLATURE

c_p, heat capacity at constant pressure;
d, cavity depth;
g, gravity vector;
Gr, Grashof number $[\equiv g(\cos\gamma)\beta\rho^2 L^3 \Delta T/\mu^2;\ \Delta T = T_w - T_0]$;
h, heat transfer coefficient;
H, channel width;
k, thermal conductivity;
l, total channel length;
l_{ds}, downstream channel length;
l_{us}, upstream channel length;
L, reference length (here $L = w$);
$\overline{Nu}$, mean Nusselt number ($\equiv \bar{h}w/k$);
Nu_X, local Nusselt number ($\equiv h_X w/k$);
p, pressure;
Pr, Prandtl number ($\equiv \mu c_p/k$);
Re, Reynolds number ($\equiv \rho \bar{V}_{in} w/\mu$);
T, temperature;
T_0, reference temperature, taken as T_{in};
T_w, temperature at cavity back-wall;
$\bar{V}_{in}$, mean velocity of inlet flow;
$\mathbf{V}$, vector velocity;
w, cavity width;
x, coordinate direction along channel length;
X, dimensionless longitudinal coordinate (x/w);
y, coordinate direction transverse to channel length;
Y, dimensionless transverse coordinate (y/w).

Greek symbols

β, thermal expansion coefficient;
γ, channel inclination angle with respect to vertical;
θ, dimensionless temperature $[\equiv (T_w - T)/(T_w - T_0)]$;
μ, viscosity;
ρ, density.

Mathematical symbols

∇, vector form of gradient operator;
∇^2, Laplacian operator.

Subscripts

X, refers to local value;
in, refers to inlet condition.

INTRODUCTION

The physical problem

THE PROBLEM of heat transfer to confined flows past open cavities relates to various engineering configurations including flat plate solar energy collectors, solar central thermal receiver systems, ventilation and fire control in buildings and cooling of elec-

*Present address: Solar Energy Research Institute, Golden, CO 80401, U.S.A.

tronic components. A number of studies prior to 1967 have been reviewed by Chilcot [1]. Other studies of these flows are also available in [2–5]. Most of the work conducted to date deals with turbulent or high Mach number regimes. While some heat transfer studies have been performed for low speed flows [6], to our knowledge, there has not yet been a systematic evaluation of the magnitude of, and role played by, free-convection effects as a function of channel inclination angle and cavity orientation.

This study represents a computational effort to bridge, in part, the information gap existing in the literature.

Geometry and flow conditions

The geometry of interest is shown in Fig. 1 and consists of a steady two-dimensional confined laminar flow in a channel which has a square cavity recessed into one of the two walls. Both the inclination angle of the channel, γ, and the orientation of the cavity are variables in the study. For example, Fig. 1 shows the channel with $\gamma = 0°$ and with the cavity recessed into the right-hand wall. For a $\gamma = 45°$, the channel would be inclined to the right and the cavity would then have an upward-facing orientation. On the other hand, for a channel inclination of $\gamma = -45°$, the channel would lean to the left and the cavity would have a downward-facing orientation. Other important parameters are the Reynolds, Prandtl, and Grashof numbers of the flow, cavity aspect ratio (d/w), channel to cavity width ratio (H/w), upstream channel length to cavity width ratio (l_{us}/w), downstream channel length to cavity width ratio (l_{ds}/w), channel flow direction, and entrance velocity profile shape.

In all calculation cases only the back wall of the cavity was heated with the remaining walls of the geometry being treated as adiabatic. Two types of entrance flow profiles were considered corresponding to uniform and parabolic (developed channel flow) shapes, respectively.

Primarily due to cost considerations, calculations were limited to the following conditions: $Re = 300$, $Gr = 4500$, $Pr = 0.709$, $(T_w - T_0)/T_0 = 0.015$, $l_{us}/w = 4$, $l_{ds}/w = 8$, $l/w = 13$, $H/w = 3$ and $d/w = 1$. It should be remarked that for these values, buoyant effects may be expected to be negligible in the channel ($Gr/Re^2 \simeq 0.05$) but pronounced within the cavity ($Gr/Re^2 \simeq 30$ from the calculations).

CALCULATION PROCEDURE

Transport equations and boundary conditions

The set of approximate elliptic* transport equations governing the flow are:

continuity

$$\nabla \cdot \mathbf{V} = 0 \tag{1}$$

momentum

$$\rho \mathbf{V} \cdot \nabla \mathbf{V} = -\nabla p + \mu \nabla^2 \mathbf{V} - \rho \frac{T - T_0}{T_0} \mathbf{g} \tag{2}$$

energy

$$\rho c_p \mathbf{V} \cdot \nabla T = k \nabla^2 T. \tag{3}$$

The boundary conditions imposed in this study are indicated in Fig. 1. It should be noted that the assumption $T_0 = T_{in}$ produced negligible errors in the calculations therefore T_{in} was used as the reference temperature in this study.

The Boussinesq approximation [7] has been used to characterize buoyant effects in the above equations and the question arises as to its validity in the context of this work. Gray and Giorgini [7] have determined that, for air, the most limiting parameters for applying the approximation are the maximum temperature difference $(T - T_0)_{max}$ and the macroscopic length scale L_{max}, both of which appear in the Grashof number. For the present case, $(T_w - T_0)/T_0 = 0.015$ and is much less than the maximum permissible value of 0.1 derived by Gray and Giorgini. Likewise, $L = w = 0.02$ m in this study and is much less than the L_{max} of 10^3 m found from the relation $\rho g L/p \leqslant 0.1$ given by these authors.

Solution procedure

The TEACH-2E [8] numerical procedure, with modifications to include the Boussinesq approximation, was used to compute solutions to the problem specified above for differing channel inclination angles, cavity orientation and flow entrance profiles. The calculation scheme has been extensively documented (in for example, [9, 10]) and only a very brief outline concerning the nature of the procedure is provided here.

Implicit finite difference equations for velocity, temperature and a pressure correction are derived by volume integration of the differential transport equations over discrete volume elements, or cells, into which the calculation domain is subdivided. The sets of equations so derived are solved line-by-line using a tri-diagonal matrix algorithm, until the whole calculation domain has been swept. Several sweeps are performed per iteration, and iteration ceases when a pre-established convergence criterion is met. Under-relaxation of the computed variables was found to improve the rate of convergence but no special measures were required to ensure stability of the numerical scheme due to the coupling between energy and momentum equations. Abdelmeguid and Spalding [11] have made a similar observation in relation to the computation of free-forced convection in inclined-pipe turbulent flow.

Validation

While validation of the numerical scheme is desir-

* While the bulk of the flow in the channel is parabolic in nature (with respect to the coordinate x) that in the cavity recirculates and requires a solution of fully elliptic equations. Elliptic equations were solved over the entire flow domain.

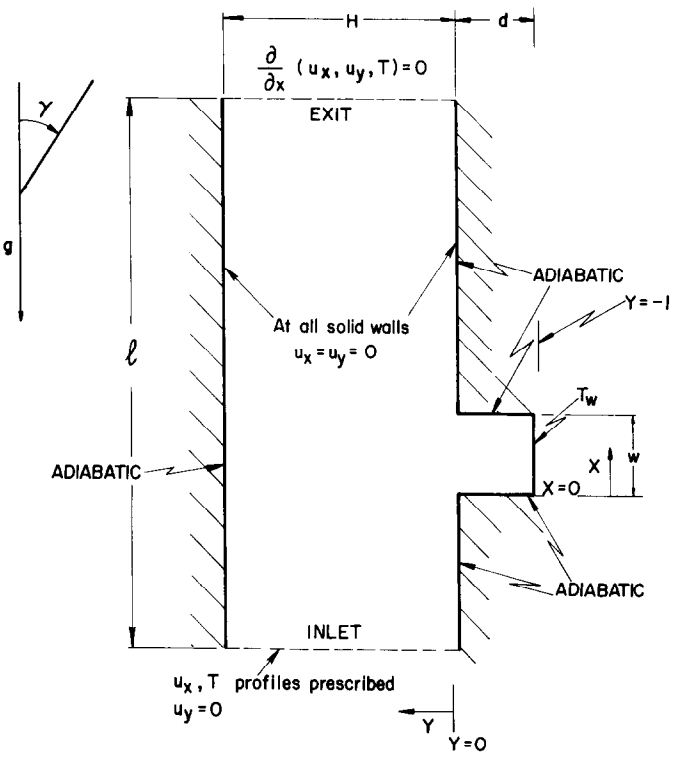

FIG. 1. Geometrical configuration showing inclination angle γ with respect to gravity vector and boundary conditions.

able, it was made difficult due to the lack of data on mixed convection flows in two-dimensional, open cavities. Nevertheless, two related test cases were calculated to check that the modified calculation procedure would predict correctly various characteristic features anticipated in the confined-channel heated-cavity flow. The first case involved the combined hydrodynamic and thermal entrance region between horizontal flat plates [12–15]. The second case is more relevant to the problem at hand and pertains to the heat transfer experiment performed by Johnson and Dhanak [6] in a two-dimensional rectangular cavity in the lower one of two horizontal parallel plates. Although not shown here, both cases showed excellent agreement between calculations and available data. Detailed comparisons will be found in Jacobs [16].

Because both of the above test cases represent flows in the forced convection regime, modifications incorporated into the calculation scheme to predict buoyant effects were not tested directly. Nevertheless, the tests provide an indirect proof that buoyant terms were properly formulated in the equations.

CASE STUDIES

Preliminary considerations

The first case study to be performed corresponds to a vertically aligned channel ($\gamma = 0°$) with an upwardly directed parabolic inlet velocity profile. This case served to determine the optimum grid refinement in the cavity for adequate resolution of the velocity and temperature fields; further refinement of the grid did not result in significantly improved predictions. Using the optimized cavity grid, a second series of calculations was performed to determine the minimum upstream and downstream channel lengths (l_{us} and l_{ds}) yielding entrance and exit-length independent solutions within the cavity.

Unequal grid spacing outside the cavity was used in the calculations to economize on the total number of grid nodes while still resolving adequately the flow in regions with strong variations of temperature and velocity, particularly in the cavity. A cavity grid refinement of 16×16 nodes, and values of $l_{us} = 4w$ and $l_{ds} = 8w$, respectively, were found to yield accurate results essentially independent of these parameters. In each case, the flow field was covered by a mesh consisting of 48 grid nodes in the x-direction and 32 in the y-direction. Typical calculation times for a converged solution on a CDC 7600 computer were approximately 70–90 CPU s.

In addition to the case studies to be discussed below, two extra sets of calculations were performed to provide a clear indication of the relative influence of cavity geometry and buoyant forces on the flow. Thus, for each one of the case studies, the overall heat transfer rate was determined with the cavity absent ($d/w = 0$), and for both types of inlet velocity profile conditions calculations neglecting buoyant effects altogether were performed. Physically, the latter results

(cases A and B in Table 1) correspond to a flow free of gravitational or body forces and, therefore, channel inclination, cavity orientation and main flow direction do not influence the results.

RESULTS AND DISCUSSION

Typical velocity vector diagrams and temperature contours corresponding to three of the calculated case studies are shown in Figs. 2–4. A comparison between Figs. 2 and 3 illustrates the effect that cavity orientation has on the flow while a comparison between Figs. 2 and 4 illustrates the directional influence of the flow. It is clearly obvious from the vector diagrams that when buoyant forces are aligned with the main flow through the channel (Figs. 2 and 3) the result is for two relatively large recirculation zones to appear within the cavity. This is due to the shearing action of the channel flow on the flow in the cavity which is primarily driven by thermal effects. As shown in Table 1, the doubly recirculating flow reduces heat transfer from the cavity back wall.

The temperature profiles corresponding to buoyant forces and main flow opposed (Fig. 4) show the strong influence that the channel flow has in reinforcing the cavity flow. The result is for hot fluid to leave the cavity near the top while cold fluid enters through the bottom.

Due to stable stratification of the flow in the cavity with a channel orientation of $\gamma = -45°$ (Fig. 3), buoyant forces affect the flow less and the main flow in the channel induces a larger recirculation zone in the cavity than it does for $\gamma = 45°$. This results in a reduced heat transfer from the cavity back wall, as shown in Table 1.

Similar results using uniform entrance velocity profiles were also calculated. Due to space limitation they are not presented here but may be found in [16] where both temperature and velocity profiles are provided.

It should be noted that the non-buoyant flow calculations corresponding to cases A and B revealed small corner vortices within the cavity as found in [6] which were not present in any of the buoyant flow calculation cases.

A summary of the overall heat transfer results for the case studies is given in Table 1. Columns 2–4 contain the permutation, for each case study, of the flow parameters. Columns 5 and 6 list the mean Nusselt numbers obtained with and without the cavity, respectively, for each flow condition. The Nusselt number was determined from the equation

$$\overline{Nu} = \frac{\bar{h}w}{k} = \frac{1}{w}\int_0^w Nu_X \, dX = \frac{1}{n}\sum_{i=1}^{n} Nu_X^i \qquad (4)$$

where n is the number of grid nodes immediately adjacent to the heated surface. The value of Nu_X was given by the dimensionless temperature gradient at the heated wall, i.e.

$$Nu_X = \left.\frac{\partial \theta}{\partial Y}\right|_{X, Y=-1} \qquad (5)$$

where $\theta = (T_w - T)/(T_w - T_0)$, $Y = y/w$, and $X = x/w$. The final column in the table shows the percentage of heat transfer from the cavity relative to that determined in the absence of the cavity.

Plots of dimensionless local Nusselt numbers

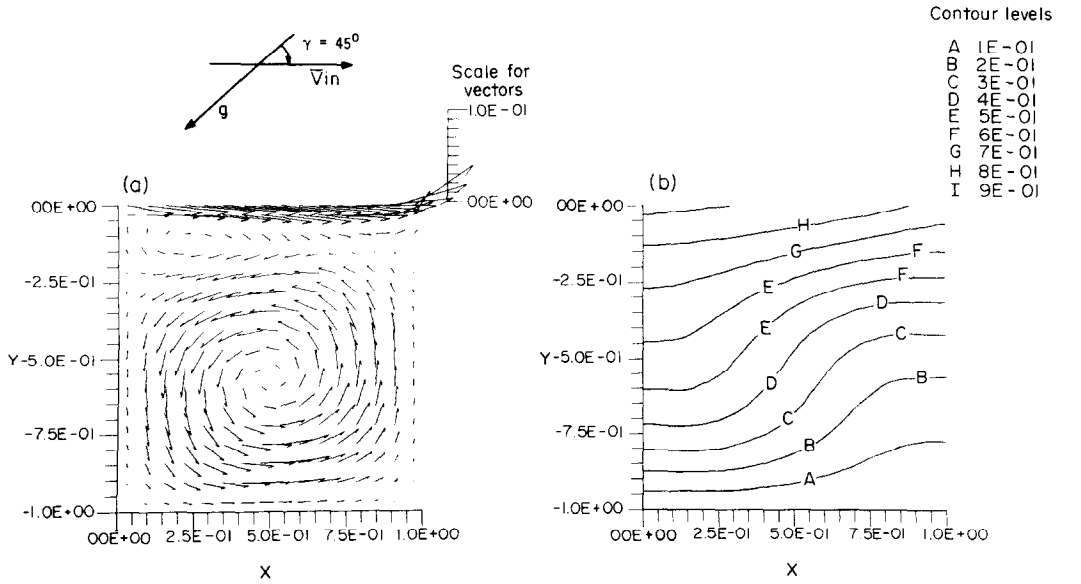

FIG. 2. Dimensionless vector velocity $\mathbf{V}/\bar{V}_{in}$ (a) and temperature θ contour (b) plots for upward-directed parabolic velocity inlet profile to a channel with $\gamma = 45°$ (case 2).

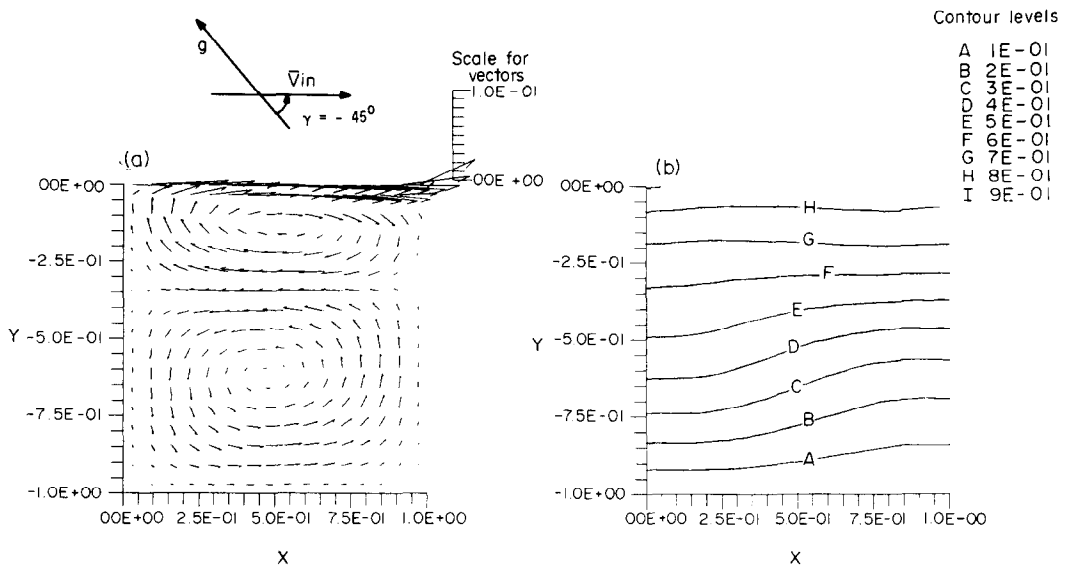

FIG. 3. Dimensionless vector velocity $\mathbf{V}/\bar{V}_{in}$ (a) and temperature θ contour (b) plots for upward-directed parabolic velocity inlet profile to a channel with $\gamma = -45°$ (case 3).

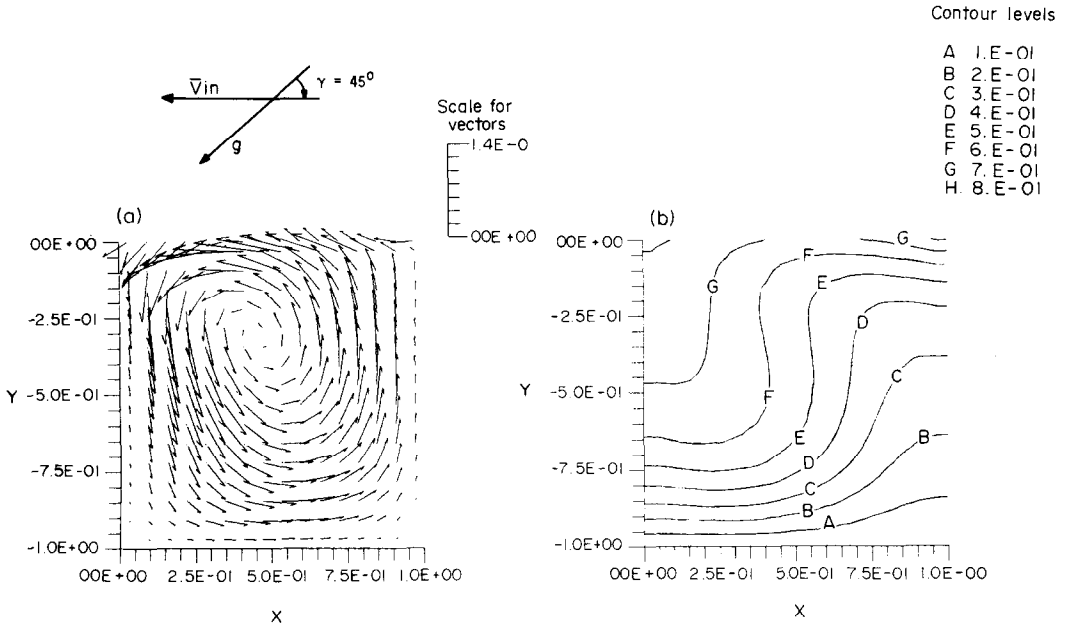

FIG. 4. Dimensionless vector velocity $\mathbf{V}/\bar{V}_{in}$ (a) and temperature contour (b) plots for downward-directed parabolic velocity inlet profile to a channel with $\gamma = 45°$ (case 5).

$(Nu_X/\overline{Nu})$ as a function of X are shown in Figs. 5 and 6 for parabolic inlet velocity profile conditions. Each figure shows four curves, one for each channel inclination angle and a fourth curve corresponding to the non-buoyant forced convection result. In general, all cases affected by buoyant forces show decreasing rates of heat transfer from the wall to the fluid as the latter is warmed (increasing value of X). Maximum rates of heat transfer take place for values of X between 0.075 and 0.275 approximately, depending on the flow configuration. Similar results for uniform inlet velocity profiles are available in [16].

The influence of stable stratification in flows with a downward facing cavity orientation ($\gamma = -45°$) is illustrated in Fig. 5, where a significant reduction in heat transfer from the cavity back wall for $X \lesssim 0.5$

Table 1. Overall heat transfer results

Case		Main flow direction	Upstream inlet velocity profile	$\overline{Nu}$	$\overline{Nu}^*$ (No cavity)	$(\overline{Nu}/\overline{Nu}^*) \times 100$
1	0°	Upward	Parabolic	1.177	6.790	17.3
2	45°	Upward	Parabolic	1.158	6.731	17.2
3	−45°	Upward	Parabolic	0.975	6.600	14.8
4	0°	Downward	Parabolic	1.652	6.010	27.5
5	45°	Downward	Parabolic	1.744	6.160	28.3
6	−45°	Downward	Parabolic	1.302	6.094	21.4
7	0°	Upward	Uniform	1.107	8.436	13.1
8	45°	Upward	Uniform	1.158	8.390	13.8
9	−45°	Upward	Uniform	1.087	8.358	13.0
10	0°	Downward	Uniform	1.928	7.998	24.1
11	45°	Downward	Uniform	2.013	8.083	24.9
12	−45°	Downward	Uniform	1.585	8.048	19.7
A*	—	—	Parabolic	1.165	6.390	18.2
B*	—	—	Uniform	1.475	8.213	18.0

*Calculations performed in the absence of buoyant effects.

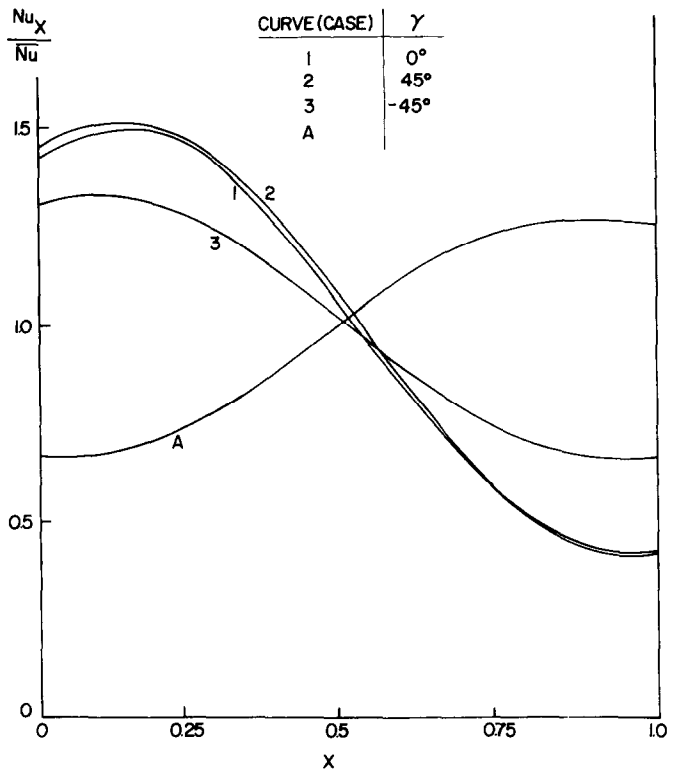

FIG. 5. Dimensionless Nusselt for upward-directed parabolic velocity inlet profile. Curve A corresponds to a flow without buoyant effects. $\overline{Nu}$ given in Table 1.

appears. Relatively small differences arise between local Nusselt number curves corresponding to $\gamma = 0°$ and 45°, respectively. A comparison between Figs. 5 and 6 suggests that stable stratification affects upward directed channel flows more strongly than it does downward directed flows. The observation is supported by corresponding values of mean Nusselt numbers listed in Table 1 and is related to the presence of two (rather than only one) recirculation zones in the case of an upward directed flow. Thus, shearing of the cavity flow at the aperture plane by the channel flow induces a recirculating motion which is countercurrent to that driven by thermal effects. This motion traps the thermally driven eddy within the cavity, thus reducing heat transfer from the back-wall.

It must be remarked that none of the flows calculated exhibited regions of flow recirculation outside the cavity and, in all cases, the cavity produced only minor effects on the main channel flow.

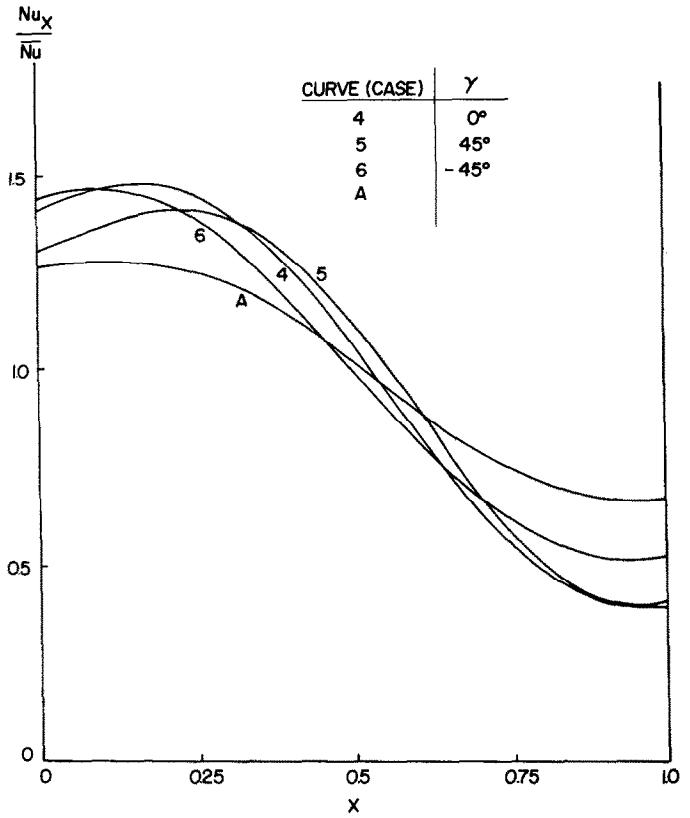

FIG. 6. Dimensionless Nusselt for downward-directed parabolic velocity inlet profile. Curve A corresponds to a flow without buoyant effects. $\overline{Nu}$ given in Table 1.

CONCLUSIONS

Although of limited extent, the results obtained in this study allow the following conclusions to be drawn:

(1) When the main channel flow is aligned with buoyant motions arising at the back-wall in the cavity (the case of upward channel flow), a *double*-recirculating flow regime is induced within the cavity. The recirculating zone near the back-wall is driven by thermal effects while that adjacent to the aperture plane is driven by the channel flow. The pair of recirculating zones produce a 'blanketing' effect in that together they act to diminish heat transfer from the cavity back-wall to the outer flow.

(2) When the main channel flow is opposed to buoyant motions arising at the back-wall in the cavity (the case of downward channel flow) a *single*-recirculating flow regime is induced within the cavity. The shearing action of the channel flow on that within the cavity at the aperture plane reinforces the back-wall thermally induced motion. From Table 1 it is clear that the effect is stronger for the uniform inlet profile case than it is for the parabolic profile case; presumably due to the more intense shearing of the flow in the aperture plane.

(3) In general, only small differences appeared between heat transfer calculations corresponding to a pair of flows with $\gamma = 0°$ and 45° respectively, the remaining calculation conditions being identical. This suggests that mixed convection heat transfer from upward-facing ($\gamma > 0°$) two-dimensional rectangular cavities is essentially independent of channel inclination. By contrast, corresponding downward-facing cavity ($\gamma = -45°$) flow calculations showed marked reductions in heat transfer. The tendency towards stable stratification in downward-facing ($\gamma < 0°$) cavity flows is the cause for a reduction in heat transfer and is a strong effect regardless of inlet profile characteristics or flow direction in the channel.

Acknowledgements—One of the authors (E.W.J.) wishes to acknowledge financial support received from the Department of Mechanical Engineering, University of California, Berkeley during the course of this work. Partial funding for the numerical computations performed at the Lawrence Berkeley Laboratories was made available through Sandia Laboratories, Contract No. 20-1012. We are grateful for this support. The authors' names on the front of the paper are in alphabetical order.

REFERENCES

1. R. E. Chilcot, A review of separating and reattaching flows with heat transfer, *Int. J. Heat Mass Transfer* **10**, 783–797 (1967).

2. R. A. White, Some results on the heat transfer within resonating cavities at subsonic and supersonic Mach numbers, *J. Basic Engng. Trans. ASME* **93,** 537–542 (1971).
3. R. L. Haugen and A. M. Dhanak, Heat transfer in turbulent boundary-layer separation over a surface cavity, *J. Heat Transfer* **89,** 335–340 (1967).
4. H. Yamamoto, N. Seki and S. Fukusako, Forced convection heat transfer on heated bottom surface of a cavity, *J. Heat Transfer* **101,** 475–479 (1979).
5. E. Chin, D. Rafiinejad and R. A. Seban, Prediction of flow and heat transfer in a rectangular wall cavity with turbulent flow, *J. Appl. Mech.*, ASME, Paper No. 72-APM-Q (1973).
6. R. W. Johnson and A. M. Dhanak, Heat transfer in laminar flow past a rectangular cavity with fluid injection, *J. Heat Transfer* **98,** 226–231 (1976).
7. D. G. Gray and A. Giorgini, The validity of the Boussinesq approximation for liquids and gases, *Int. J. Heat Mass Transfer* **19,** 545–551 (1976).
8. A. D. Gosman and W. M. Pun, Lecture notes for course entitled: calculation of recirculating flows, Imperial College Report No. HTS/74/2, London University (1974).
9. S. V. Patankar, *Numerical Heat Transfer and Fluid Flow.* McGraw-Hill (1980).
10. J. A. C. Humphrey, Numerical calculation of developing laminar flow in pipes of arbitrary curvature radius, *Can. J. Chem. Engng* **56,** 151–164 (1978).
11. A. M. Abdelmeguid and D. B. Spalding, Turbulent flow and heat transfer in pipes with buoyancy effects, *J. Fluid Mech.* **94,** 383–400 (1979).
12. R. K. Shah and A. L. London, *Advances in Heat Transfer. Supplement* 1, *Laminar Forced Convection in Ducts*, pp. 190–195. Academic Press (1978).
13. W. E. Mercer, W. M. Pearce and J. E. Hitchcock, Laminar forced convection in the entrance region between parallel flat plates, *J. Heat Transfer* **99,** 251–257 (1967).
14. J. R. Bodoia and J. F. Osterle, Finite difference analysis of plane Poiseuille and Couette flow development, *Appl. Sci. Res.* **10,** 265–276 (1961).
15. E. M. Sparrow, S. H. Lin and T. S. Lundgren, Flow development in the hydrodynamic entrance region of tubes and ducts, *Physics Fluids* **7,** 338–347 (1964).
16. E. W. Jacobs, Natural and forced convection in laminar flow past a two-dimensional, rectangular cavity, M.Sc. Thesis Report, Dept. Mech. Eng., Univ. of Calif., Berkeley (1980).

CONVECTION THERMIQUE LAMINAIRE MIXTE POUR UNE CAVITE CARREE DANS UN CANAL, AVEC UNE INCLINAISON VARIABLE

Résumé—On étudie numériquement, à partir des équations selon Boussinesq, la convection thermique mixte laminaire pour une cavité carrée dans un canal avec une inclinaison variable. Toutes les parois sont adiabatiques à l'exception de la paroi arrière, dans la cavité, qui est à une température constante plus élevée que celle de l'écoulement à l'entrée. L'influence sur le transfert thermique de l'orientation de la cavité, de l'inclinaison de la cavité, de la direction de l'écoulement et du profil à l'entrée a été étudiée pour des conditions d'écoulement qui correspondent à $Pr = 0{,}709$, $Re = 300$ et $Gr = 4500$, basée sur la largeur de la cavité, le débit moyen et l'angle d'orientation de la cavité, $\gamma = 0$ correspondant à un écoulement vertical.

Les calculs montrent que des forces de pesanteur significatives apparaissent dans la cavité quand $Gr/Re^2 = 30$, mais qu'elles sont faibles dans le canal où $Gr/Re^2 = 0{,}05$. En général, les calculs montrent des flux thermiques accrus quand les forces de gravité sont opposées à la direction pricipale de l'écoulement et des flux réduits quand elles sont dans la même direction.

Une stratification stable de l'écoulement dans la cavité tournée vers le bas est responsable de la réduction du transfert thermique par rapport au cas de la cavité tournée vers le haut avec les conditions d'écoulement semblables.

Bien que limités à un domaine étroit de caractéristiques géométriques et dynamiques, et dans le cadre des approximations de Boussinesq, les résultats montrent clairement les rôles relatifs et les ordres de grandeur de ces effets et ils devraient être utiles aux chercheurs intéressés par l'influence des forces d'Archimède induites par les mouvements dans les écoulements en conduite.

DER WÄRMEÜBERGANG BEI LAMINARER FREIER KONVEKTION VON EINEM QUADRATISCHEN HOHLRAUM IN EINEN KANAL MIT VERÄNDERBARER NEIGUNG

Zusammenfassung—Der Wärmeübergang bei laminarer freier Konvektion von einem quadratischen Hohlraum in einen Kanal mit veränderbarer Neigung wurde unter Verwendung von Boussinesq-Näherungsgleichungen numerisch untersucht. Alle Wandflächen der geometrischen Anordnung waren adiabat mit Ausnahme der Rückwand des Hohlraumes. Diese wurde auf einer konstanten Temperatur gehalten, die höher lag als die der ankommenden Strömung. Der Einfluß der Orientierung des Hohlraumes, der Kanalneigung, der Strömungsrichtung und des Eintrittsprofils wurden für Strömungsbedingungen mit den folgenden Kennzahlen untersucht: $Pr = 0{,}709$; $Re = 300$ und $Gr = 4500$; Bezugsgrößen waren dabei die Hohlraumbreite, der mittlere Massenstrom und ein Hohlraumorientierungswinkel γ, wobei $\gamma = 0$ senkrechter Kanalströmung entspricht. Die Berechnungen zeigen, daß nennenswerte Auftriebskräfte im Hohlraum auftreten, wenn $Gr/Re^2 \simeq 30$ ist, daß sie jedoch klein sind für $Gr/Re^2 \simeq 0{,}05$. Allgemein ergeben die Berechnungen einen verstärkten Wärmeübergang, wenn die Auftriebskräfte entgegen der Hauptströmungsrichtung wirken, und einen verminderten Wärmeübergang, wenn sie gleichsinnig wirken. Eine stabil geschichtete Strömung bei abwärts-orientierter Hohlraum-Geometrie ist verantwortlich für einen verschlechterten Wärmeübergang, verglichen mit aufwärts-orientierter Geometrie unter gleichwertigen Strömungsbedingungen. Obwohl die Anwendung der Boussinesq-Näherung auf einen engen Bereich der geometrischen und dynamischen Kenngrößen beschränkt ist, zeigen die mitgeteilten Ergebnisse eindeutig die relativen Beiträge und Größenordnungen dieser Effekte und sollten daher wertvoll für Forscher sein, die sich mit dem Einfluß auftriebsbedingter Bewegungen in geführten Strömungen befassen.

КОНВЕКТИВНЫЙ ТЕПЛОПЕРЕНОС ОТ КВАДРАТНОЙ ПОЛОСТИ В КАНАЛЕ С ПЕРЕМЕННЫМ УГЛОМ НАКЛОНА В УСЛОВИЯХ СВОБОДНОЙ И ВЫНУЖДЕННОЙ ЛАМИНАРНОЙ КОНВЕКЦИИ

Аннотация — В приближении Буссинеска численно исследуется теплоотдача от прямоугольной полости в канале с переменным углом наклона в условиях свободной и вынужденной конвекции. Все стенки геометрической конфигурации являются адиабатическими за исключением задней стенки полости, температура которой поддерживается постоянной и превышающей температуру потока на входе. Исследуется влияние на теплоперенос ориентации полости, угла наклона канала, направления течения и входного профиля при следующих значениях параметров потока: $Pr = 0{,}709$, $Re = 300$ и $Gr = 4500$. Безразмерные параметры построены по ширине полости, средней скорости потока при угле ориентации полости $\gamma = 0$ и условиях течения, соответствующих режиму течения в вертикальном канале.

Результаты расчетов свидетельствуют о том, что в полости с $Gr/Re^2 \simeq 30$ возникают большие подъемные силы, в то время как в канале с $Gr/Re^2 \simeq 0{,}05$ эти силы незначительны. В целом, результаты расчетов показывают, что когда подъемные силы действуют в сторону, противоположную направлению основного потока, перенос тепла усиливается, а когда оба направления совпадают — снижается. При прочих равных условиях течения в конфигурациях с нагревательной полостью, расположенной в верхней горизонтальной стенке канала, из-за устойчивой стратификации потока в полости наблюдается снижение интенсивности переноса тепла по сравнению со случаем, когда нагревательная полость расположена в днище канала.

Несмотря на то, что результаты исследования ограничены узким диапазоном геометрических и динамических характеристик, для которых справедлива аппроксимация Буссинеска, они дают ясное представление об относительной роли и величине этих эффектов, а поэтому должны представлять интерес для тех, кто исследует влияние подъемных сил на течение в канале.